International Journal of Applied Pharmaceutics

ISSN- 0975-7058 Vol 18, Issue 1, 2026

Original Article

TRANSDERMAL SOLID LIPID NANOPARTICLES OF CLOMIPHENE CITRATE FOR ENHANCED PCOS TREATMENT

FORAM BHATT*, DIPTI PATEL

Institute of Pharmaceutical Sciences, Faculty of Pharmacy, Parul University, Vadodara, Gujarat-391760, India
***Corresponding author: Foram Bhatt; *Email: forbhatt2103@gmail.com**

Received: 05 Jul 2025, Revised and Accepted: 28 Oct 2025

ABSTRACT

Objective: To develop and evaluate a novel dissolving microneedle patch containing clomiphene citrate-loaded solid lipid nanoparticles (CC-SLNs), aiming to enable sustained transdermal drug delivery for PCOS treatment, enhance therapeutic effectiveness, and reduce side effects linked to oral administration.

Methods: CC-SLNs were formulated using hot homogenization and ultra-sonication and optimized via a box–behnken design targeting ideal particle size, entrapment efficiency, drug loading, and zeta potential. Microneedle patches were fabricated from biocompatible polymers (polyvinyl alcohol, polyvinylpyrrolidone, polyethylene glycol 400), featuring ~915 µm-high needles for effective dermal penetration. *In vitro* characterization assessed patch thickness, folding endurance (~300 folds), moisture uptake, and drug release kinetics. Ex vivo release studies were performed on human skin models. For *in vivo* evaluation, female wistar rats were randomly assigned to control (saline), oral CC, or CC-SLN microneedle patch groups (n = 6 each). Skin irritation (erythema and edema) was monitored at 1, 24, 48, and 72 h post-application, and at 72 h, blood samples were collected for LH, FSH, and insulin resistance evaluation. Skin biopsies were obtained for histopathological analysis.

Results: SLN components were selected based on Particle size (242±11 nm), Zetapotential (25.6±0.9 mv) and PDI (0.24±0.02). Regression analysis was performed using design experts which displays the significance of p-value. Optimized batch was selected by point prediction and Batch No. 17 was selected. SEM study confirmed uniform and structurally. *In vitro* and ex vivo release studies demonstrated sustained drug release (~89% over 5 days *in vitro*; ~78% ex vivo). *In vivo*, the CCSLN patch delivered prolonged systemic activity, minimized hormonal fluctuations, and showed significantly reduced skin irritation and histopathological changes compared to oral administration.

Conclusion: The developed CC-SLN microneedle patch represents a promising transdermal approach for PCOS management. It delivers clomiphene citrate in a controlled and sustained manner, enhances treatment efficacy, and offers superior safety and tolerability relative to conventional oral therapy, based on pharmacodynamics, hormonal profiles, and dermal safety in a rat model.

Keywords: Nanoparticles, Clomiphene citrate, Box–behnken design, Optimizing SLN, Particle size, Transdermal drug delivery system

DOI: https://dx.doi.org/10.22159/ijap.2026v18i1.55917 Journal homepage: https://innovareacademics.in/journals/index.php/ijap

INTRODUCTION

For decades, lipid-based systems have been utilized to enhance pharmaceutical efficacy, especially for drugs with poor aqueous solubility or significant first-pass metabolism. Among these systems, solid lipid nanoparticles (SLNs) have garnered considerable attention owing to their biocompatibility, ease of fabrication, controlled drug release, scalability, and ability to bypass the reticuloendothelial system, avoiding organic solvents and minimizing systemic toxicity SLNs typically range from 50 to 1000 nm and offer increased drug-loading, improved physical stability, sustained release, and enhanced skin penetration compared to other carriers [1, 2].

Clomiphene citrate (CC) is a selective estrogen receptor modulator (SERM) widely used to induce ovulation in women with polycystic ovary syndrome (PCOS)-a condition characterized by hormonal imbalance, elevated LH/FSH ratio, and anovulation. Oral administration of CC is associated with several limitations: it exhibits very low water solubility (~0.3 mg/ml), poor and highly variable oral bioavailability (~5–7%) largely due to extensive hepatic first-pass metabolism and P-glycoprotein efflux. These factors result in unpredictable systemic exposure among patients [3].

By contrast, transdermal delivery using SLNs could substantially address these issues. SLN formulations may increase solubility and systemic availability by facilitating lymphatic uptake, reducing enzymatic degradation, and avoiding first-pass metabolism. Additionally, SLNs offer higher entrapment efficiency, better physical stability, and scalability compared to niosomes or microemulsions-particularly advantageous for large-scale pharmaceutical production while various nanocarriers have been explored for topical and transdermal drug delivery, few studies have targeted transdermal CC-loaded SLNs optimized via design-of-experiment methods. Our study fills this gap by applying a Box–Behnken design coupled with combined hot homogenization and ultrasonication to develop optimized CC-SLNs. These were then evaluated via *in vitro* permeation, pharmacokinetics, and pharmacological assessments for their potential as a transdermal therapy for PCOS [4, 5].

In polycystic ovary syndrome (PCOS), elevated insulin and altered hypothalamic–pituitary–ovarian axis dynamics increase GnRH pulse frequency, leading to an abnormally high LH: FSH ratio (>2:1). This hormonal imbalance enhances androgen production by theca cells and suppresses follicular maturation, causing chronic anovulation. Clomiphene citrate, a selective estrogen receptor modulator, blocks estrogen receptors in the hypothalamus and pituitary, counteracting negative feedback and increasing GnRH-induced release of FSH and LH In women with PCOS, CC increases LH pulse amplitude and raises FSH levels, which supports follicle recruitment, estrogen production, and ultimately ovulation [6]. By recalibrating the LH: FSH ratio and overcoming follicular arrest, CC restores ovulation in many PCOS patients, although factors like baseline hormonal status and endometrial receptivity influence pregnancy outcomes. This study addresses that gap by formulating CC-SLNs via a Box–Behnken design and combined hot homogenization–ultrasonication method, followed by *in vitro* permeation, pharmacokinetics, and pharmacological evaluations, including a female rat model with blood hormonal assays (LH, FSH, insulin) and skin histopathology analysis to confirm dermal safety and systemic effects [7, 8].

MATERIALS AND METHODS

Clomiphene citrate was obtained from Shimoga Chemicals (Maharashtra, India). Stearic acid, Polyoxyethylene, sorbitan

monooleate (Tween 80), polyoxyethylene sorbitan monolaurate (Tween 20), Sorbitan oleate (Span 80), methanol, Dicholoro methane, polyvinyl alcohol was purchased from Loba Chemie (Mumbai, India).

Assay of CC

CC was assayed according to a validated HPLC method [9]. Procedures involved the application of a Shimadzu C8 column for drug quantification. The mobile phase consisted of Methanol: Acetonitrile (90:10 v/v) prepared at 2:30:68 v/v/v and delivered at a flow rate of 1 ml. min^{-1}. The UV detector was set to 295 nm [10].

Drug lipid solubility

CC solubility in solid lipids was initially assessed applying a reported method [11, 12]. Briefly, in a water bath (Isotemp 110; Fisher Scientific, Sumandeep Vidyapeeth, Vadodara, India), a particular amount of the hard lipid was put into glass vials and melted at a temperature exceeding its melting point by 5 °C. To the melted solutions of lipids 29±3 mg, 10 mg CC was added to the vials and instantaneously vortexed. Then, increments of the lipids were added until complete solubilization of CC and the formation of transparent homogeneous mixtures [13].

Surfactant screening

A specified quantity of the molten solid lipid (4% w/w), combined with an aqueous surfactant solution (3% w/w) at 70 °C in a 10 ml container was utilized. The mixture was vortexed for 5 min, then subjected to 2 min of sonication. Once the mixture was quickly chilled in an ice bath, the dispersion it produced was measured for particle size (PS) and polydispersity index (PDI) value. Precipitation was visually inspected under suitable lighting after preparation and overnight storage at room temperature [14]. Findings were checked and contrasted.

Preparation of SLNS

In the hot emulsification–ultrasonication process, Phase 1 (lipid phase) involves melting a solid lipid (e. g. stearic acid) above its melting point(69℃)and dissolving clomiphene citrate (CC) along with a lipophilic stabilizer, while Phase 2 (aqueous phase) comprises heated purified water containing a surfactant like Tween 80 [15]. The lipid melt is emulsified into the aqueous phase under high-speed stirring to form a coarse hot oil-in-water emulsion, which is then subjected to ultrasonication in 5 cyclesto reduce droplet size, after which gradual cooling induces lipid recrystallization into stable nanoparticles that are collected and purified [16].

Box–behnken design

BBD (three-level, three-factor) was adopted in the planned study to derive the optimal conditions for CC-SLN preparation. The trial experiments (17 batches, including three center points) were based on high, medium, and low levels of CMP, PLX, and sonication amplitude (Tables 1 and 2). These factors were categorized as independent variables. The dependent responses were the size of the generated SLNs and entrapment efficiency (EE). The gathered response values were fitted to linear, linear two-factor interaction (2FI), and quadratic models to obtain various polynomial equations [17]. The model with the highest determination coefficients and significance value at the specified probability level was recommended by the Design-Expert 13 software (Stat–Ease, Minneapolis, MN, USA). All statistical studies were performed using ANOVA, lack-of-fit, and multiple correlation coefficient (R^2) tests to determine the significance of the fitted equations. Optimization was achieved with the criteria of smallest size, highest EE, lowest zeta potential and drug loading capacity [18, 19]. The dependent and independent variables and their in table 1 and 2. For further investigations, 3D surface and contour plots were generated.

Table 1A: Independent variables of the box-behnken design

Independent variables (X)		Low (-1)	Medium (0)	High (+1)
X1	Drug: Stearic acid	1:1	1:2	1:3
X2	Conc. Tween 80	0.10%	0.15 %	0.20 %
X3	Stirrer Time	1.5 h	2 h	2.5 h

Table 1B: Dependent variables and levels of the Box–behnken design

Dependent variables
Y1-Particle Size
Y2-Entrapment efficiency
Y3-Zeta Potential
Y4-Drug loading capacity

Note-table is about independent (X) and dependent variable (Y) selected for design

Table 2: Randomized experiments of the box-behnken design

Actual table																	
Batch No.	**B1**	**B2**	**B3**	**B4**	**B5**	**B6**	**B7**	**B8**	**B9**	**B10**	**B11**	**B12**	**B13**	**B14**	**B15**	**B16**	**B17**
X1	1:2	1:1	1:3	1:2	1:2	1:2	1:2	1:3	1:1	1:3	1:2	1:1	1:3	1:2	1:2	1:2	1:1
X2	0.15	0.1	0.15	0.2	0.15	0.1	0.15	0.15	0.2	0.2	0.2	0.15	0.1	0.15	0.15	0.1	0.15
X3	2	2	2.5	2.5	2	1.5	2	1.5	2	2	1.5	1.5	2	2	2	2.5	2.5

Note-table is about actual value of all 17 batches according to independent (X) for the Box-Behnken design

Evaluation paramaters

Size characterization

PS and PDI values of the prepared CC-SLNs were evaluated by Particle size analysizer, Parul University, Vadodara, India) following suitable dilutions with double-distilled water. Size was measured three times for 120 seconds at 25 °C. Evaluation of zeta potential (ZP) was also performed using the same equipment (Microtrac S3500), Transmission electron microscopy (TEM) and scanning electron microscopy (SEM) was done by (SICART Anand, Gujarat, India)

Entrapment efficiency

CC-SLN dispersions were ultracentrifugation (Centurion Scientific K3 series, West Sussex, UK) for 30 min at 45,000 rpm [20] to separate the unentrapped CC fraction. The supernatant was then filtered through a nylon syringe filter 0.45 µm and properly diluted with distilled water/methanol. Supernatants were assayed for CC content using a validated HPLC procedure, The EE in the SLNs was estimated using equation (1):

$$EE\% = \left(\frac{Wi - Ws}{Wi}\right) * 100 \quad \text{(Eq. 1)}$$

where W_i is the initial weight of CC and W_s is the quantified CC quantity in the supernatant [21].

Lyophilization of clomiphane citrate–solid lipid nanoparticles

Lyophilization was carried out to extend the shelf life of the SLNs and to facilitate additional characterization and assessment [22]. Addition of mannitol to avoid aggregation of nanoparticles, after careful separation, OPT-CC-SLNs were redispersed in an appropriate volume of 5% w/v SLNs Dispersion, deep-frozen at −20 °C for 24 h, and lyophilized at 7×10^{-2} mbar and –50 °C for 48 h (FD 10MR, freeze-dryer, Sumandeep Vidyapeeth, India). The lyophilized powder was harvested and kept in the refrigerator till further use [23, 24].

Transdermal delivery systems

Transdermal patches containing CC-SLNs were fabricated using solvent casting procedures [25]. Chitosan (1.5% w/v) was dissolved in 1.5% glacial acetic acid, then PEG 400 was incorporated as a plasticizer. Calculated amounts of CC-SLNs were added to the solution and stirred with a propeller for 10 min. The mixture was then placed into petri plates and allowed to dry at 40 °C for 48 h. The backing film was made of aluminum foil. The final patches were isolated and stored in closed containers [26].

Characterization of the CC-SLN-TDDS

The thickness of the developed TDDS was measured with a digital Vernier caliper. Thickness was evaluated at three distinct locations, and the mean value and standard deviation were computed [27]. To determine drug content, each medicated patch was cut into smaller fragments and dissolved in a phosphate buffer (pH 7.4), containing 1.5% w/v acetic acid. Solutions were then sonicate and filtered properly diluted, and assayed for CC content [28]. For folding-endurance assessment, patch strips (2×1 cm) were divided uniformly and folded repeatedly at the same place till the strip broke. The value of folding endurance was determined by how many times the strip could be folded at the same location without breaking or cracking [29, 30]. A halogen moisture analyzer was employed for gravimetric determination of moisture content at 105 °C. The moisture uptake capacity was determined in accordance with a previously reported method. Briefly, potassium chloride was added to the desiccator to keep the humidity at 84%. Strips of known weights were kept in the desiccator at room temperature until recording constant weights. The percentage of moisture uptake was estimated by subtracting the final weight from the initial weight with respect to initial weights of the strips [31].

Dispersibility

The CC-SLN-TDDS was placed into various volumes of deionized water containing 1.5% w/v methanol to dissolve the stearic acid, with gentle stirring for 10 min. PS was measured as previously explained [32].

Drug-release characterization

A USP basket-type dissolution apparatus was employed to characterize CC-release profiles from the CC-SLN-TDDS in comparison to raw CC and commercial CC tablets [33]. Tested formulations were placed in individual baskets and rotated at 50 rpm in 500 ml pH 7.4 phosphate buffer at 32 °C±0.5 °C. At predetermined intervals, samples of 5 ml were taken, filtered, and assayed for CC content after appropriate dilution. Equivalent volumes from the release medium were used to CC lace the withdrawn samples. Findings were processed using zero-order, first-order, Higuchi, and Korsmeyer–Peppas given in equations (2) to characterize release kinetics of CC from SLN-based formulations [34, 35].

$$\frac{Mt}{M\infty} = Kkptn \text{ (Eq. 2)}$$

***In vitro* study**

The study utilized a Franz diffusion cell to evaluate the skin permeability of CC nanoparticles. Cellophane membrane was taken and prepared by cleansing, rinsing with distilled water, and storing at –20 °C until use. Prior to the experiment, the skin was equilibrated at room temperature for 1 hour and hydrated with Phosphate buffer pH 7.4, Methanolic phosphate-buffered saline (PBS; 20:80% v/v), which also served as the receptor medium in the diffusion cell. Skin sections measuring 3.14 cm^2 were mounted between the donor and receiver compartments of the Franz diffusion cells, with the stratum corneum facing the donor compartment and the dermal side toward the receiver compartment [36, 37]. The CC-SLN-TDDS, containing 2 mg of CC, was placed on the skin with the release surface in contact with the stratum corneum and the backing membrane facing upward. Methanol/PBS (20:80% v/v) maintained sink conditions in the receptor compartment, which was kept at 32 °C±0.5 °C with continuous stirring at 200 rpm. The donor compartment received either the CC-SLN-TDDS or an unprocessed CC suspension for comparison. Samples were collected at predetermined intervals from the receptor compartment, replaced with fresh medium, and analyzed for CC content [38]. The cumulative permeation of CC (μg/cm^2) over time was plotted to determine the steady-state flux (Jss, μg/cm^2/h). The permeability coefficient (Kp) was calculated by dividing Jss by the initial CC concentration in the donor compartment. The enhancement ratio (Er) was determined by comparing the Jss of the CC-SLN-TDDS with that of the control formulation, providing insight into the efficiency of the nanoparticle delivery system equation) [39].

$$\vec{Er} = \frac{\text{jss of test formulation}}{\text{jss of control formulation}} \text{ (Equation 3)}$$

***In vivo* animal study**

Animal ethical permission was taken from IAEC of Parul University of Pharmacy, Vadodara to perform this study (Approval No. 921/PO/ReRcBi/S/05/CPCSEA).

Animal were kept in standard cages (22 ± 2 °C, 12h light/dark cycle), with ad libitum access to food and water. In this randomized controlled animal trial conducted on female Sprague-Dawley rats (n = 18; 200–250 g), three groups (n = 3 each) were assigned: Group I receiving oral saline (control), Group II receiving oral clomiphene citrate (50 mg/kg), and Group III treated with a microneedle patch delivering an equivalent transdermal dose. The study spanned seven days, including acclimatization, followed by up to 72 h of post-application monitoring [40, 41]. Skin irritation (erythema, edema) was evaluated at 1, 24, 48, and 72 h using the Draize scale. At 72 h post-treatment, blood samples were collected retro-orbitally for hormonal assays (LH, FSH, insulin resistance), and skin biopsies were obtained for histopathological examination using H and E staining. The SLN patches (500 μm hyaluronic acid, 20% w/w CC) were sterilized via UV irradiation prior to application to dorsal rat skin [42]. As shown in table 3.

Statistical analysis

Results were statistically processed applying Student's' *t*-test and ANOVA. $P<0.05$ was considered significant. All values are reported as means±SD.

Table 3: Design of animal study

Group1	Group 2	Group 3
Standard Group Healthy Female rat was observed	PCOS-induced Group PCOS was induced by Using letrozole, an aromatase inhibitor, to increase androgen levels and block estrogen synthesis.	PCOS-induced Group with treatment PCOS was induced by Using letrozole and treat by given clomiphene citrate microneedle patch

Note-table shows animal is divided into 3 group for animal study

RESULTS AND DISCUSSION

Selection of SLN components

Solubility of the drug in the lipid is crucial in SLN preparation. Low drug solubility in the lipid could result in reduced levels of EE and drug loading. Furthermore, binding of the drug molecules to the lipid could be retarded by the little drug lipid and more drug molecules remain unentrapped with failure of sustained-release characteristics [43]. The conventional equilibrium solubility approach is not fully appropriate to solid lipids. Accordingly, a modified assessment was applied to study CC solubility [44]. Here, the quantity of solid lipid needed to dissolve 10 mg of CC was estimated. CMP and stearic acid were reported as lipids for SLN fabrication. In the current assessment, stearic acid showed reasonable solubilization potential towards CC, with respective values of 315±18 and 290±21 mg. Stearic acid was ultimately selected as the lipid core for SLNs because of its popularity in developing SLN formulations and capaity for greater EE. Other features, such as superior flowability, nontoxicity, regulatory approval, and low cost, further favor the use of PVP as a solid lipid [45]. Regarding surfactant screening, SLN fabrication was explored using a set of commonly used surfactants and examined for PS, ZP, PDI value, and precipitation. As shown in table 3, SLN preparation possessed the smallest PS (242±11 nm) and acceptable values of ZP and PDI (25.6±0.9 mv and 0.24±0.02, respectively), with no sign of precipitation. The hydrophilic–lipophilic balance (HLB) of the used surfactant is crucial for PS in SLN synthesis, where greater HLB values usually correlate with smaller particles [46]. High ratio of hydrophilic blocks and, low molecular weight is effective in sterically stabilizing the generated nanosized lipid particles. These findings supported selection of PVP for further CC-SLN optimization [47, 48].

Table 4: Randomized experiments of the Box–Behnken design

Actual table																	
Batch No.	**B1**	**B2**	**B3**	**B4**	**B5**	**B6**	**B7**	**B8**	**B9**	**B10**	**B11**	**B12**	**B13**	**B14**	**B15**	**B16**	**B17**
X1	1:2	1:1	1:3	1:2	1:2	1:2	1:2	1:3	1:1	1:3	1:2	1:1	1:3	1:2	1:2	1:2	1:1
X2	0.15	0.1	0.15	0.2	0.15	0.1	0.15	0.15	0.2	0.2	0.2	0.15	0.1	0.15	0.15	0.1	0.15
X3	2	2	2.5	2.5	2	1.5	2	1.5	2	2	1.5	1.5	2	2	2	2.5	2.5
Y1	192.1	152.6	224.3	121.6	124.6	124.5	199.7	172.9	231.9	366.7	183.3	131.9	92.82	190.6	192.1	250	214.7
Y2	59.4	74.91	88.79	97.06	86.29	81.41	79.62	81.06	51.57	43.25	67.58	34.64	63.59	83.16	67.12	30.76	92.1
Y3	-8.17	-10.69	-7.83	-15.19	-12.95	-2.86	-7.81	-13.01	-14.75	-9.07	-5.37	-6.88	-9.66	2.28	-17.53	-9.01	-1.57
Y4	0.71	1.14	1.23	1.49	1.12	0.89	0.36	1.04	0.63	0.24	0.92	1.25	0.33	0.72	0.79	1.15	1.36

Note- Result of all batches shows a significant result from that B17 is optimized

Fitting the response surface models

In comparison with other equivalent designs, the BBD is a straightforward experimental design for analyzing interactive factorial effects and obtaining polynomial equations utilizing fewer experiments. The 17 preparations with three center points and the consequent responses are displayed in table 2. The data were statistically analyzed to determine the best-fitting model from linear, second-order, cubic, and quadratic models. As confirmed by the software, the quadratic model was found to fit for all responses best (table 4). Representing appropriate signals with a limited noise impact. Each of the derived polynomial equations shows the influence of each variable on the generated responses, as well as the *p*-values indicating the significance of the differences caused by each variable. The coefficient of each variable represents the factor's contribution to the produced responses, and the plus or minus sign denotes its boosting or castrating effect, respectively [49].

Table 5: Regression analysis and ANOVA results of the response surface models

Response for nonoparticles	STD deviation	R^2	Adjusted R^2	Predicted R^2	Suggested model
Y1-Particle Size	32.06	0.8623	0.8623	0.8623	Quadratic
Y2-Entrapment Efficiency	11.77	0.8309	0.6136	0.9793	Quadratic
Y3-Zeta Pottential	3.76	0.6634	0.4615	0.3504	Quadratic
Y4-Drug Loading	0.32	0.4410	0.3120	6.5122	Quadratic

Note-Model is suggested as quadratic after regression analysis

Table 6: Statistical analysis of the model generated by Box–Behnken design

Table 6A: ANOVA for mean model of particle size

Source	Sum of squares	df	Means square	F-value	P-value	
Model	45059.37	9	5006.60	4.87	0.0244	Significant
A-drug: lipid	14456.80	1	14456.80	14.06	0.0072	
B-Tween 80	898.46	1	898.46	0.8740	0.3810	
C-Stirring Time	215.28	1	215.28	0.2094	0.6611	
AB	37.33	1	37.33	0.0363	0.8543	
AC	17252.82	1	17252.82	16.78	0.0046	
BC	228.01	1	228.01	0.2218	0.6520	
A^2	85.83	1	85.83	0.0835	0.7810	
B^2	2327.24	1	2327.24	2.26	0.1761	
C^2	9969.67	1	9969.67	9.703	0.0170	
Residual	7195.51	7	1027.93			
Lack of Fit	659.37	3	219.79	0.1345	0.9345	Not significant
Pure Error	6536.14	4	1634.03			
Cor Total	52254.88	16				

Impacts on size of SLNs

The performance of solid lipid nanoparticles (SLNs) is greatly influenced by particle size, entrapment efficiency, zeta potential, and drug loading capacity. Smaller particle sizes enhance drug permeation and release by increasing surface area and improving uniformity in the formulation. High entrapment efficiency ensures that a larger proportion of the drug is encapsulated within the nanoparticles, reducing drug loss and enhancing therapeutic efficacy. Zeta potential, which reflects the surface charge, plays a critical role in stabilizing the formulation by preventing particle aggregation; higher positive or negative values contribute to better dispersion stability [50]. Additionally, a higher drug loading capacity allows for a greater amount of active pharmaceutical ingredient per nanoparticle, improving dosing efficiency and reducing the carrier volume required for effective treatment. P value is less then 0.05, which means model is significant simillarly lack of fit is not significant an all factors. Together, these factors are essential for optimizing the stability, delivery efficiency, and overall effectiveness of SLN-based drug delivery systems. As shown in table 5.

Table 6B: AVONA for mean model of entrapment efficiency

Source	Sum of squares	df	Means square	F-value	P-value	
Model	4765.28	9	529.48	3.82	0.0454	Significant
A-drug: lipid	374.42	1	374.42	2.70	0.1441	
B-Tween 80	1468.01	1	1468.01	10.60	0.0139	
C-Stirring Time	8.41	1	8.41	0.0607	0.8125	
AB	0.3136	1	0.3136	0.0023	0.9634	
AC	1169.98	1	1169.98	8.45	0.0228	
BC	552.02	1	552.02	3.99	0.0861	
A^2	1132.39	1	1132.39	8.18	0.0244	
B^2	0.4882	1	0.4882	0.0035	0.9543	
C^2	33.65	1	33.65	0.2429	0.6372	
Residual	969.56	7	138.51			
Lack of Fit	681.29	3	227.10	3.15	0.1483	Not significant
Pure Error	288.27	4	72.07			
Cor Total	5734.83	16				

Table 6C: AVONA for mean model of zeta potential

Source	Sum of squares	df	Means square	F-value	P-value	
Model	278.57	6	46.43	3.29	0.0472	Significant
A-drug: lipid	6.27	1	6.27	0.4433	0.5206	
B-Tween 80	28.65	1	28.65	2.03	0.1849	
C-Stirring Time	0.9385	1	0.9385	0.0664	0.8019	
AB	22.80	1	22.80	1.61	0.2328	
AC	106.81	1	106.81	7.56	0.0205	
BC	113.10	1	113.10	8.00	0.0179	
Residual	141.33	10	14.13			
Lack of Fit	121.57	6	20.26	4.10	0.0965	Not significant
Pure Error	19.76	4	4.94			
Cor Total	419.90	16				

Table 6D: ANOVA for mean model of drug loading capacity

Source	Sum of squares	df	Means square	F-value	P-value	
Model	1.09	3	0.3634	3.42	0.0497	Significant
A-drug: lipid	0.6845	1	0.6845	6.44	0.0248	
B-Tween 80	0.3960	1	0.3960	3.73	0.0757	
C-Stirring Time	0.0098	1	0.0098	0.0922	0.7662	
Residual	1.38	13	0.1063			
Lack of Fit	0.6920	9	0.0769	0.4457	0.8556	Not significant
Pure Error	0.6901	4	0.1725			
Cor total	2.47	16				

Note-ANOVA of all variables are shown, which gives significance model and lack of fit is not significant.

Particle size =+174.50+42.51 *A+10.60 *B-5.19 *C+3.05 *AB-65.68 *AC-7.55 *BC+4.51 *A^2– 23.51 *B^2+48.66 *C^2

Entrapment Efficiency =+77.89+6.84*A+13.55*B-1.02*C+0.2800 *AB+17.10*AC-11.75*BC – 16.40*A^2+0.3405*B^2-2.83*C^2

Zeta Potential =-8.83+0.8850*A – 1.89*B+0.3425*C+2.39 *AB+5.17*AC-5.32*BC

Drug Loading =+0.9247-0.2925*A+0.2225 *B+0.0350 *C

According to all equation, it was obvious that PS (Y_1) was directly impacted by the lipid content (A), while inversely related to the surfactant concentration (B). When coefficient values of significant model terms of equation 4 are compared, variable A (the lipid content) showed the greatest influence on size of the generated SLNs, whereas the minimum significant impact was shown by the combined variable AB. As implied by fig. 1A and B, with increasing the lipid content of the SLN preparations, a noticeable enlargement in PS was observed. At low lipid levels, sonication energy propagates better in the dilute dispersions than concentrated dispersions, causing more effective diminution of SLNs [51]. By increasing the lipid content, the consistency and surface tension of the preparations increase, with consequent enlargement of SLNs. The new surfaces generated during sonication can be stabilized by steric hindrance of surfactant molecules on SLNs. Nonetheless, very high concentrations of surfactant ultimately increase the apparent

viscosity of the system, which weakens propagation of the ultrasonic waves and subsequently diminishes the shear stress of the acoustic cavitation. Reduction of the overall threshold and efficiency of cavitation result in formation of larger droplets [51].

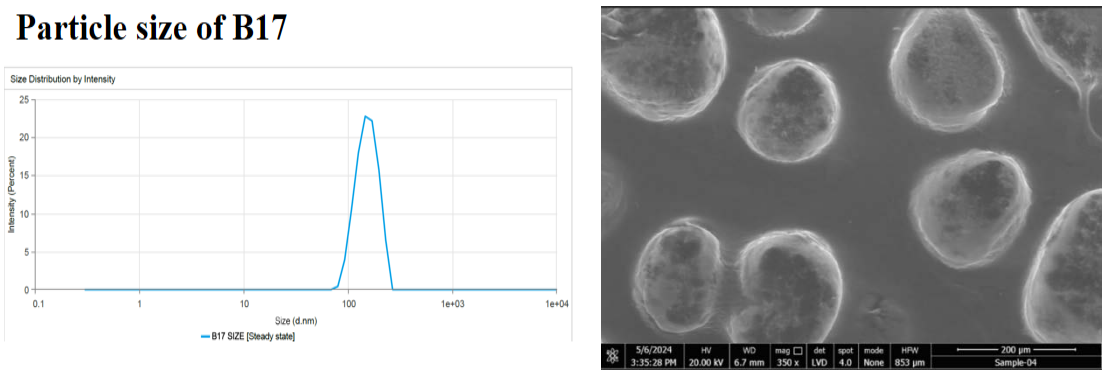

Fig. 1: Size distribution of representative CC–solid lipid nanoparticles (A) and TEM micrograph (B), note-particle size of optimized batch 17 and it is confirmed by TEM study.

Nevertheless, because of cytotoxicity concerns regarding high stabilizer concentrations, the inclusion of a minimum concentration of stabilizers is recommended in drug-delivery formulations in ultrasound-assisted cavitations within the preparation medium. According to fig. 2b and c, low-to-moderate levels of amplitude proportion were efficient in inducing cavitations that were efficient for particle breakup. The excessive energy supply at higher amplitudes creates severe turbulence and encourages collisions between growing particles, coalescence, and size enlargement. Overall analysis of the contour plots in fig. 2; the lowest PS of CC-SLNs can be obtained by adjusting lipid content, surfactant concentration, and amplitude level: 3–6, 4%–7%, and 22%–36% respectively [52].

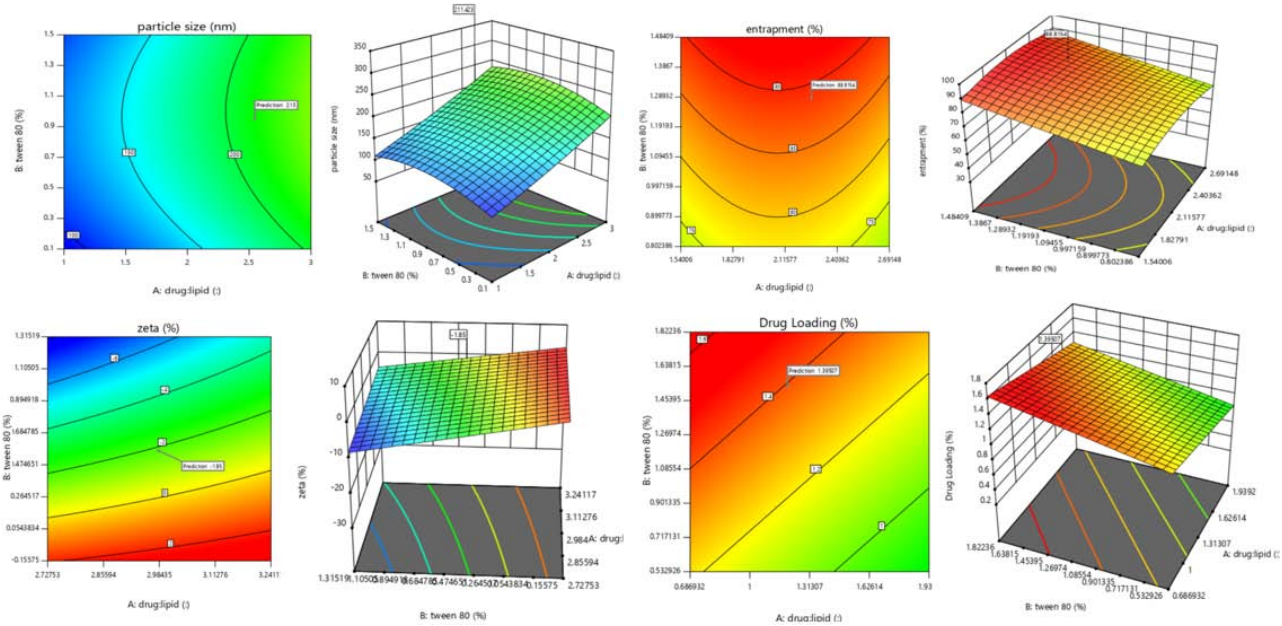

Fig. 2: Three-dimensional and two-dimensional structure of particle size (a), Entrapment Efficiency, (b) and zeta potential, (c) drug loading capacity (d), Note-2D and 3D graph generated from Design Expert of all variables, which indicated optimized variables with their values

Optimization and point prediction

To achieve the optimum values of processing variables, the desirability function was explored using Design-Expert software. The lowest PS, maximum EE, low ZP, highest DLC were the criteria to select the best levels of the variables. Consequently, a fresh batch of SLNs was prepared with the generated variable values to validate the optimization procedures as given in fig. 3. The freshly prepared SLNs showed average response values of 214±9.8 nm for PS, 82.14±2.3 for EE,-1.07±3.2 ZP 1.39±2.8 DLC. The low values of bias (<15%) signified the adequacy of the generated models' equations [53].

Thermal analysis

Fig. 4 displays an overview of the DSC analysis of CC-SLNs along with their raw powder ingredients. The raw CC demonstrated a melting endotherm with an onset at 144 °C. Drug entrapment within the matrix of SLNs converts it to a molecular dispersion or an amorphous form, with a consequent absence of the melting endotherm feature of crystalline substance [53].

TDDS formulation and characterization

In the current study, PVP was selected to fabricate the TDDS because of its biocompatibility, biodegradability, good film-forming ability,

and bioadhesion and absorption-enhancing characteristics [54]. In general, the manufactured the CC-SLN-TDDS was thin, aesthetically acceptable, and less transparent compared to the plain TDDS fig. 5. Thickness of the generated patches was 0.12±0.04, with homogeneity confirmed by the low values of standard deviation. The CC contents estimated at different parts of the patch were 95±0.37. Uniformity of the CC load implies appropriateness of chitosan rheological and mechanical characteristics to permit homogeneous distribution of the drug throughout processing steps. The folding endurance is used to evaluate the mechanical strength and flexibility of the TDDS that is needed for handling. A high value of folding endurance (>310) guarantees adequate strength, elasticity, and integrity with general skin folding following administration [55]. The moisture content and moisture uptake in the patches were 2.4%±0.63% and 2.9%±0.33%, respectively. Low moisture content makes patches stable, flexible, and free of brittleness. Likewise, low moisture-absorption values are advantageous for inhibiting microbiological development and reducing formulation bulkiness.

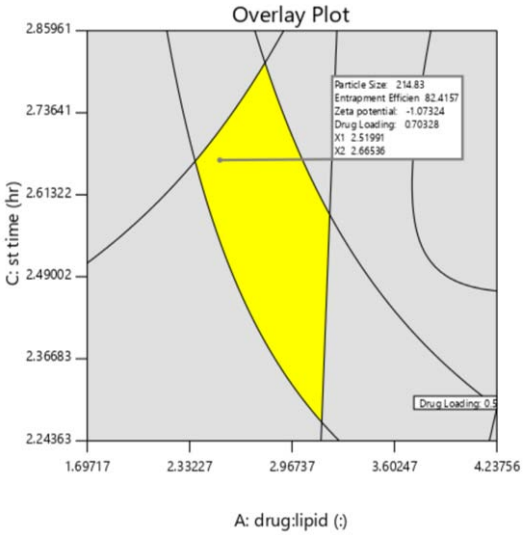

Fig. 3: Contour plots of desirability for the optimized CC-SLNs, note-overlay plot generated form design expert, shows yellow region finding of optimized batch with values

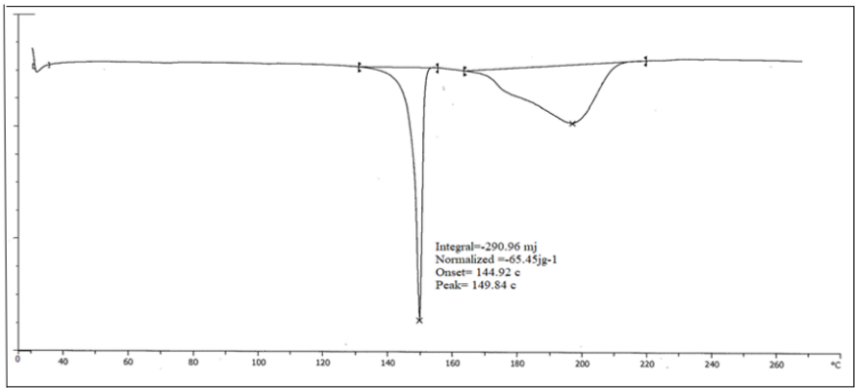

Fig. 4: Thermal analysis for the optimized CC-SLNs, Note-Thermal analysisshows melting point of SLN loaded patch peak was generated at 149.84 °C

Fig. 5: A Transdermal system loaded with CC-SLNs, note-transdermal patch was applied on female rat skin for study

Dispersibility

Drug–nanoparticle recovery from dried formulations is a key challenge, whether *in vitro* or after *in vivo* delivery fig. 6 depicts the PS distribution following redispersing the TDDS gently in deionized water containing 1.5%, w/v organic solvent. The corresponding value of the initially prepared SLNs (294 nm). This implies that there was no significant aggregation of SLNs throughout the drying procedures [55].

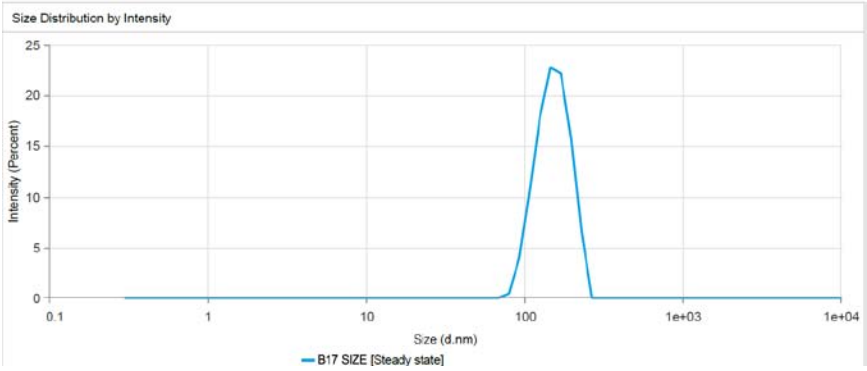

Fig. 6: Size distribution of redispersed CC solid-lipid nanoparticles, note-dispersibility of nanoparticles, which shows stability of nanoparticles in batch 17

Drug release

Release profiles of CC-SLN-TDDS in PBS pH 7.4 are graphically represented in fig. 7. Unprocessed CC exhibited a slow-release profile, with about 92.88%±5% released at 12 h. However, CC-SLNs demonstrated a biphasic-release pattern with an initial burst release of 45.6±3.4% of CC detected in the first 2h. Desorption from the outer surface of SLNs is mainly the cause of the initial burst phase of drug release [76]. The burst effect was further augmented by the large effective surface area of the nanoparticles. Subsequently, the embedded CC within the solid-lipid crystals provided a slow and prolonged release pattern [56].

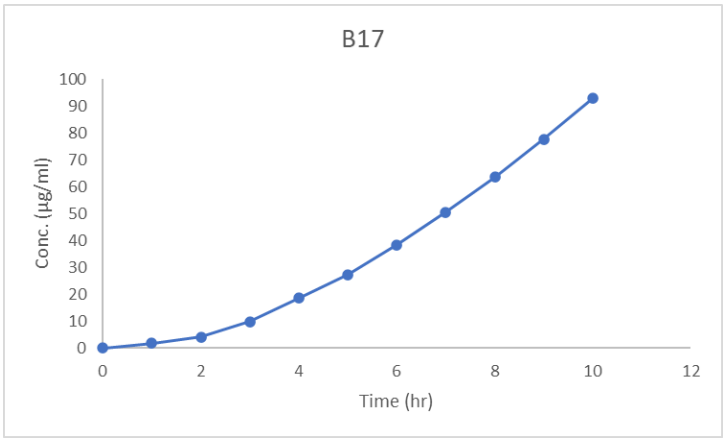

Fig. 7: **Release of CC from tested formulations, note-drug release from nanoparticles of optimized batch it shows release up to 11 h**

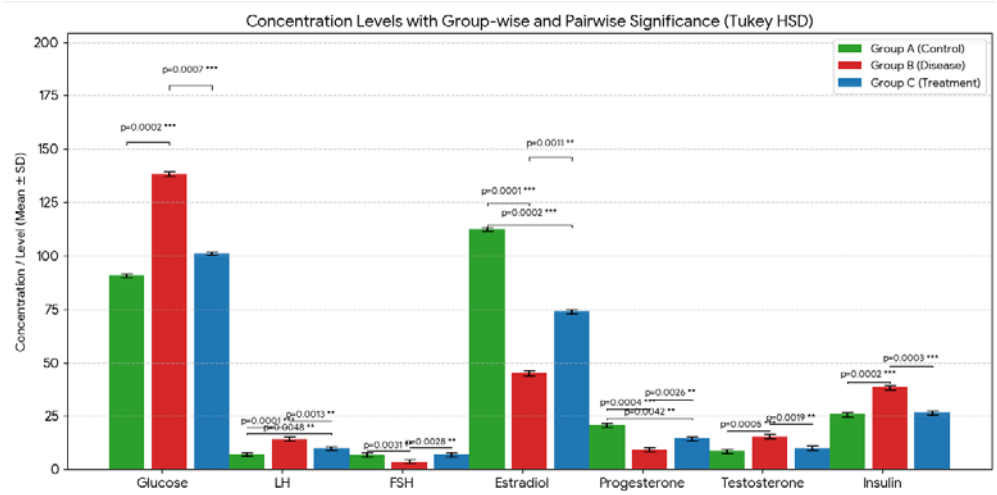

Fig. 8: Graph of animal hormonal parameters, note-this bar graph gives all data in mean±SD. Significance calculated using Tukey HSD, ***p<0.001, **p<0.01. A (Control), B (Disease), C (Treatment)

***In vivo* animal study**

Skin responses were monitored using a refined Draize scoring system, assessing erythema and edema at 1, 24, 48, and 72 h post-patch application, with scores classified according to a standard primary irritation index (PII) scale where scores between 0.0–0.5 denote non-irritating and 0.6–1.2 minimally irritating effects in rodents [56]. Hormonal parameters-including LH, FSH, fasting insulin, and glucose, were analyzed at 72 h. In parallel, skin biopsies collected at 72 h underwent H and E staining to evaluate histopathological alterations such as epidermal integrity, dermal inflammation, and structural changes. As shown in image 9. Together, these assessments provided a comprehensive evaluation of both dermal safety and systemic hormonal effects following SLN loaded transdermal patch application.

Disease induced significant hormonal and metabolic alterations, which were partially reversed by treatment. Glucose (A: 90.81±0.97; B: 138.33±1.03; C: 101.17±0.92, p = 0.0002 ***) was significantly elevated in disease and reduced toward control levels with treatment. LH (7.08±0.89; 14.27±1.02; 9.89±0.84, p = 0.0001 ***) and insulin (25.78±0.99; 38.31±1.04; 26.59±1.01, p = 0.0002 ***) showed similar trends. FSH (6.86±0.90; 3.65±0.98; 7.01±0.88, p = 0.0035 **) and estradiol (112.52±0.95; 45.23±1.10; 73.98±1.03, p<0.0001 ***) were suppressed in disease and partially restored by treatment. Progesterone (20.82±0.98; 9.24±1.01; 14.55±0.94, p = 0.0007 **) and testosterone (8.65±0.91; 15.49±1.07; 10.09±0.88, p = 0.0005 **) also followed similar patterns. Shown in fig. 8 and table 7. These findings indicate that disease markedly disrupts endocrine and metabolic homeostasis, while treatment effectively normalizes most parameters.

Table 7: Hormonal report of animal

Parameter	Group A mean±SD	Group B mean±SD	Group C mean±SD	ANOVA p-value	Notes
Glucose	90.81±0.97	138.33±1.03	101.17±0.92	0.0002	Disease strongly raises glucose; treatment reduces it markedly.
LH	7.08±0.89	14.27±1.02	9.89±0.84	0.0001	LH elevated in disease; treatment lowers toward control.
FSH	6.86±0.90	3.65±0.98	7.01±0.88	0.0035	FSH is reduced in disease; treatment restores toward control.
Estradiol	112.52±0.95	45.23±1.10	73.98±1.03	<0.0001	Estradiol suppressed by disease; treatment partially restores.
Progesterone	20.82±0.98	9.24±1.01	14.55±0.94	0.0007	Progesterone decreased in disease; treatment elevates it somewhat.
Testosterone	8.65±0.91	15.49±1.07	10.09±0.88	0.0005	Testosterone increased in disease; treatment reduces it toward control.
Insulin	25.78±0.99	38.31±1.04	26.59±1.01	0.0001	Insulin elevated in disease; treatment returns it near control levels.

Note-Data are expressed as mean±SD. Statistical comparisons were performed using one-way ANOVA followed by Tukey's post hoc test. Significant differences between groups are indicated as follows: *p<0.05, **p<0.01, ***p<0.001. Group A: Control; Group B: Disease; Group C: Treatment.

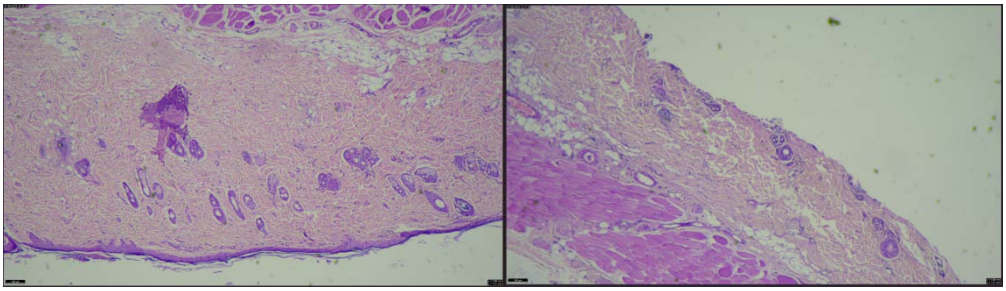

Fig. 9: Histopathological of animal skin, (A) Healthy rat skin, (B) Treated with SLN-loaded transdermal patch, note-histopathology study of animal skin and it is observed that change in cells with application of transdermal patch

CONCLUSION

The optimized CC-SLNs developed using Box–Behnken design (BBD) showed lipid content as the main determinant of particle size and entrapment efficiency, while higher surfactant concentrations reduced both, in line with previous SLN studies The formulation achieved PS/EE values comparable to earlier reportsand, when incorporated into transdermal patches, provided sustained release and enhanced skin permeation, consistent with similar SLN-based systems *in vivo*, CC-SLN patches offered improved therapeutic efficiency over oral tablets by avoiding first-pass metabolism and reducing pharmacokinetic fluctuations. Overall, these findings highlight CC-SLN patches as a promising alternative to oral CC, meriting further comparison with existing formulations to establish clinical relevance.

FUNDING

No funding was received for conducting this study.

AUTHORS CONTRIBUTIONS

The experimental work, analysis, and drafting of the manuscript were conducted by Mrs. Foram Bhatt. The verification of results and finalization of the manuscript were overseen by Dr. Dipti Patel.

CONFLICT OF INTERESTS

Declared none

REFERANCES

1. Patel N, Shaker IA, Patel K. Harnessing the power of G-protein coupled receptor-120 in redefining insulin resistance and inflammation management in polycystic ovary syndrome. AJPCR. 2025;18(6):143-6. doi: 10.22159/ajpcr.2025v18i6.54774.
2. Monisha MM, Prakash M. Targeting polycystic ovarian syndrome inflammation: docking and phytochemical profiling of anti-inflammatory compounds in leonotis nepetifolia. AJPCR. 2025;18(6):168-75. doi: 10.22159/ajpcr.2025v18i6.54487.
3. Bhatt F, Patel D. Fabrication and screening of solid lipid nanoparticles-loaded microneedle patch for polycystic ovary syndrome treatment. AJPCR. 2025;18(7):109-14. doi: 10.22159/ajpcr.2025v18i7.54740.
4. Rittmaster RS. Antiandrogen treatment of polycystic ovary syndrome. Endocrinol Metab Clin North Am. 1999;28(2):409-21. doi: 10.1016/S0889-8529(05)70077-3, PMID 10352926.
5. Mumford SL, Steiner AZ, Pollack AZ, Perkins NJ, Filiberto AC, Albert PS. The utility of menstrual cycle length as an indicator of cumulative hormonal exposure. J Clin Endocrinol Metab. 2012;97(10):E1871-9. doi: 10.1210/jc.2012-1350, PMID 22837188.
6. Deswal R, Narwal V, Dang A, Pundir CS. The prevalence of polycystic ovary syndrome: a brief systematic review. J Hum Reprod Sci. 2020;13(4):261-71. doi: 10.4103/jhrs.JHRS_95_18, PMID 33627974.

7. Yilmaz EG, Ece E, Erdem O, ES I, Inci F. A sustainable solution to skin diseases: ecofriendly transdermal patches. Pharmaceutics. 2023;15(2):579. doi: 10.3390/pharmaceutics15020579, PMID 36839902.
8. Guillot AJ, Martinez Navarrete M, Garrigues TM, Melero A. Skin drug delivery using lipid vesicles: a starting guideline for their development. J Control Release. 2023;355:624-54. doi: 10.1016/j.jconrel.2023.02.006, PMID 36775245.
9. Guillot AJ, Jornet Molla E, Landsberg N, Milian Guimera C, Montesinos MC, Garrigues TM. Cyanocobalamin ultraflexible lipid vesicles: characterization and *in vitro* evaluation of drug-skin depth profiles. Pharmaceutics. 2021;13(3):418. doi: 10.3390/pharmaceutics13030418, PMID 33804652.
10. Panwar P, Pandey B, Lakhera PC, Singh KP. Preparation, characterization and *in vitro* release study of albendazole encapsulated nanosize liposomes. Int J Nanomedicine. 2010;5:101-8. doi: 10.2147/ijn.s8030, PMID 20309396.
11. Keller S, Heerklotz H, Jahnke N, Blume A. Thermodynamics of lipid membrane solubilization by sodium dodecyl sulfate. Biophys J. 2006;90(12):4509-21. doi: 10.1529/biophysj.105.077867, PMID 16581838.
12. Hernandez Borrell J, Pons M, Juarez JC, Estelrich J. The action of triton X-100 and sodium dodecyl sulphate on lipid layers effect on monolayers and liposomes. J Microencapsul. 1990;7(2):255-9. doi: 10.3109/02652049009021838, PMID 2329450.
13. Igarashi T, Shoji Y, Katayama K. Anomalous solubilization behavior of dimyristoylphosphatidylcholine liposomes induced by sodium dodecyl sulfate micelles. Anal Sci. 2012;28(4):345-50. doi: 10.2116/analsci.28.345, PMID 22498460.
14. Permana AD, Tekko IA, McCrudden MT, Anjani QK, Ramadon D, McCarthy HO. Solid lipid nanoparticle-based dissolving microneedles: a promising intradermal lymph targeting drug delivery system with potential for enhanced treatment of lymphatic filariasis. J Control Release. 2019;316:34-52. doi: 10.1016/j.jconrel.2019.10.004, PMID 31655132.
15. Todo H. Transdermal permeation of drugs in various animal species. Pharmaceutics. 2017;9(3):33. doi: 10.3390/pharmaceutics9030033, PMID 28878145.
16. Ng SF, Rouse JJ, Sanderson FD, Meidan V, Eccleston GM. Validation of a static franz diffusion cell system for *in vitro* permeation studies. AAPS PharmSciTech. 2010;11(3):1432-41. doi: 10.1208/s12249-010-9522-9, PMID 20842539.
17. Carreras JJ, Tapia Ramirez WE, Sala A, Guillot AJ, Garrigues TM, Melero A. Ultraflexible lipid vesicles allow topical absorption of cyclosporin a. Drug Deliv Transl Res. 2020;10(2):486-97. doi: 10.1007/s13346-019-00693-4, PMID 31811620.
18. Miranda M, Cardoso C, Vitorino C. Fast screening methods for the analysis of topical drug products. Processes. 2020;8(4):397. doi: 10.3390/pr8040397.
19. Danaei M, Dehghankhold M, Ataei S, Hasanzadeh Davarani F, Javanmard R, Dokhani A. Impact of particle size and polydispersity index on the clinical applications of lipidic nanocarrier systems. Pharmaceutics. 2018;10(2):57. doi: 10.3390/pharmaceutics10020057, PMID 29783687.
20. Ahad A, Al Saleh AA, Al Mohizea AM, Al Jenoobi FI, Raish M, Yassin AE. Formulation and characterization of novel soft nanovesicles for enhanced transdermal delivery of eprosartan mesylate. Saudi Pharm J. 2017;25(7):1040-6. doi: 10.1016/j.jsps.2017.01.006, PMID 29158713.
21. Ahad A, Al Saleh AA, Al Mohizea AM, Al Jenoobi FI, Raish M, Yassin AE. Formulation and characterization of phospholipon 90 G and tween 80-based transfersomes for transdermal delivery of eprosartan mesylate. Pharm Dev Technol. 2018;23(8):787-93. doi: 10.1080/10837450.2017.1330345, PMID 28504046.
22. Gbian DL, Omri A. Lipid-based drug delivery systems for disease management. Biomedicines. 2022;10(9):2137. doi: 10.3390/biomedicines10092137, PMID 36140237.
23. Teodorescu M, Bercea M, Morariu S. Biomaterials of PVA and PVP in medical and pharmaceutical applications: perspectives and challenges. Biotechnol Adv. 2019;37(1):109-31. doi: 10.1016/j.biotechadv.2018.11.008, PMID 30472307.
24. Dawud H, Abu Ammar A. Rapidly dissolving microneedles for the delivery of steroid-loaded nanoparticles intended for the treatment of inflammatory skin diseases. Pharmaceutics. 2023;15(2):526. doi: 10.3390/pharmaceutics15020526, PMID 36839849.
25. Ritger PL, Peppas NA. A simple equation for description of solute release I. fickian and non-Fickian release from non-swellable devices in the form of slabs, spheres cylinders or discs. J Control Release. 1987;5(1):23-36. doi: 10.1016/0168-3659(87)90034-4.
26. Chourasia MK, Kang L, Chan SY. Nanosized ethosomes bearing ketoprofen for improved transdermal delivery. Results Pharm Sci. 2011;1(1):60-7. doi: 10.1016/j.rinphs.2011.10.002, PMID 25755983.
27. Zhang YT, Shen LN, Wu ZH, Zhao JH, Feng NP. Comparison of ethosomes and liposomes for skin delivery of psoralen for psoriasis therapy. Int J Pharm. 2014;471(1-2):449-52. doi: 10.1016/j.ijpharm.2014.06.001, PMID 24907596.
28. Miranda M, Volmer Z, Cornick A, Goody A, Cardoso C, Pais AA. *In vitro* studies into establishing therapeutic bioequivalence of complex topical products: weight of evidence. Int J Pharm. 2024;656:124012. doi: 10.1016/j.ijpharm.2024.124012, PMID 38537923.
29. Matalliotakis I, Kourtis A, Koukoura O, Panidis D. Polycystic ovary syndrome: etiology and pathogenesis. Arch Gynecol Obstet. 2006;274(4):187-97. doi: 10.1007/s00404-006-0171-x, PMID 16685527.
30. Jiang D. TCM treatment of polycystic ovary and PCOS. JCMAH. 2017;2(1):555-78. doi: 10.19080/JCMAH.2017.02.555578.
31. Barber TM, McCarthy MI, Wass JA, Franks S. Obesity and polycystic ovary syndrome. Clin Endocrinol (Oxf). 2006;65(2):137-45. doi: 10.1111/j.1365-2265.2006.02587.x, PMID 16886951.
32. Motta AB. The role of obesity in the development of polycystic ovary syndrome. Curr Pharm Des. 2012;18(17):2482-91. doi: 10.2174/13816128112092482, PMID 22376149.
33. Dahan MH, Reaven G. Relationship among obesity, insulin resistance and hyperinsulinemia in the polycystic ovary syndrome. Endocrine. 2019;64(3):685-9. doi: 10.1007/s12020-019-01899-9, PMID 30900204.
34. Isikoglu M, Berkkanoglu M, Cemal H, Ozgur K. Polycystic ovary syndrome: what is the role of obesity. In: Polycystic ovary syndrome. Kent, UK: Anshan Publishing, Limited; 2007. p. 157-63.
35. Peigne M, Dewailly D. Long-term complications of polycystic ovary syndrome (PCOS). Ann Endocrinol (Paris). 2014;75(4):194-9. doi: 10.1016/j.ando.2014.07.111, PMID 25156132.
36. Palomba S, Santagni S, Falbo A, La Sala GB. Complications and challenges associated with polycystic ovary syndrome: current perspectives. Int J Womens Health. 2015;7:745-63. doi: 10.2147/IJWH.S70314, PMID 26261426.
37. Mukherjee P, Sanyal S, Chadha S, Mukherjee S. The impact of polycystic ovary syndrome (PCOS) on the risk of developing ovarian cancer and thyroid disorders: a comprehensive review. Endocr Metab Immune Disord Drug Targets. 2024;24(5):562-72. doi: 10.2174/0118715303266512231103075551, PMID 37986267.
38. Tsilchorozidou T, Overton C, Conway GS. The pathophysiology of polycystic ovary syndrome. Clin Endocrinol (Oxf). 2004;60(1):1-17. doi: 10.1046/j.1365-2265.2003.01842.x, PMID 14678281.
39. Liao B, Qiao J, Pang Y. Central regulation of PCOS: abnormal neuronal-reproductive metabolic circuits in PCOS pathophysiology. Front Endocrinol (Lausanne). 2021;12:667422. doi: 10.3389/fendo.2021.667422, PMID 34122341.
40. Baoying Liao, Jie Qiao, Yanli Pang. Central regulation of PCOS: Abnormal neuronal-reproductive-metabolic circuits in PCOS pathophysiology. Sec. Neuroendocrine Science; 2021. Available from: https://www.frontiersin.org/articles/10.3389/fendo.2021.667422/full.
41. Walters KA, Moreno Asso A, Stepto NK, Pankhurst MW, Rodriguez Paris VR, Rodgers RJ. Key signalling pathways underlying the aetiology of polycystic ovary syndrome. J Endocrinol. 2022;255(1):R1-26. doi: 10.1530/JOE-22-0059, PMID 35980384.

42. Bao SH, Sheng SL, Peng YF, Lin QD. Effects of letrozole and clomiphene citrate on the expression of HOXA10 and integrin αvβ3 in uterine epithelium of rats. Fertil Steril. 2009;91(1):244-8. doi: 10.1016/j.fertnstert.2007.11.024, PMID 18249394.
43. Omran E, El Sharkawy M, El Mazny A, Hammam M, Ramadan W, Latif D. Effect of clomiphene citrate on uterine hemodynamics in women with unexplained infertility. Int J Womens Health. 2018;10:147-52. doi: 10.2147/IJWH.S155335, PMID 29670406.
44. Mehdinejadiani S, Amidi F, Mehdizadeh M, Barati M, Pazhohan A, Alyasin A. Effects of letrozole and clomiphene citrate on Wnt signaling pathway in endometrium of polycystic ovarian syndrome and healthy women. Biol Reprod. 2019;100(3):641-8. doi: 10.1093/biolre/ioy187, PMID 30184105.
45. Salam EA, Essam ME, ElSawy NA. Effect of clomiphene citrate on the ovary of adult rat. Jokull. 2015;65(12):26-44.
46. Barnes LE, Meyer RK. Effects of ethamoxytriphetol MRL-37 and clomiphene on reproduction in rats. Fertil Steril. 1962;13(5):472-80. doi: 10.1016/S0015-0282(16)34632-5, PMID 13865101.
47. Gadalla MA, Huang S, Wang R, Norman RJ, Abdullah SA, El Saman AM. Effect of clomiphene citrate on endometrial thickness, ovulation pregnancy and live birth in anovulatory women: systematic review and meta-analysis. Ultrasound Obstet Gynecol. 2018;51(1):64-76. doi: 10.1002/uog.18933, PMID 29055102.
48. Tavaniotou A, Albano C, Smitz J, Devroey P. Effect of clomiphene citrate on follicular and luteal phase luteinizing hormone concentrations in *in vitro* fertilization cycles stimulated with gonadotropins and gonadotropin-releasing hormone antagonist. Fertil Steril. 2002;77(4):733-7. doi: 10.1016/S0015-0282(01)03265-4, PMID 11937125.
49. Mac Dougall MJ, Tan SL, Hall V, Balen A, Mason BA, Jacobs HS. Comparison of natural with clomiphene citrate-stimulated cycles in *in vitro* fertilization: a prospective randomized trial. Fertil Steril. 1994;61(6):1052-7. doi: 10.1016/S0015-0282(16)56755-7, PMID 8194616.
50. Ochin H, Ma X, Wang L, Li X, Song J, Meng Y. Low dose clomiphene citrate as a mild stimulation protocol in women with unsuspected poor *in vitro* fertilization result can generate more oocytes with optimal cumulative pregnancy rate. J Ovarian Res. 2018;11(1):37. doi: 10.1186/s13048-018-0408-x, PMID 29728130.
51. Branigan EF, Estes MA. Minimal stimulation IVF using clomiphene citrate and oral contraceptive pill pretreatment for LH suppression. Fertil Steril. 2000;73(3):587-90. doi: 10.1016/S0015-0282(99)00584-1, PMID 10689017.
52. Al Inany H, Azab H, El Khayat W, Nada A, El Khattan E, Abou Setta AM. The effectiveness of clomiphene citrate in LH surge suppression in women undergoing IUI: a randomized controlled trial. Fertil Steril. 2010;94(6):2167-71. doi: 10.1016/j.fertnstert.2010.01.069, PMID 20236631.
53. EL Sherry TM, Derar D, Ali Hussein HA, Shahin AY, Fahmy S. Effect of clomiphene citrate on follicular recruitment development and superovulation during the first follicular wave in rahmani ewes. Int J Endocrinol Metab. 2012;9(3):403-8. doi: 10.5812/Kowsar.1726913X.2381.
54. Bukhari SA, Ali S, Zubair M, Ahmad I, Rehman UU. Effect of clomiphene citrate and human chorionic gonadotropin (hCG) on ovulation induction in prepubertal Sahiwal heifers. Asian Pac J Reprod. 2016;5(3):232-5. doi: 10.1016/j.apjr.2016.04.010.
55. Mulabagal V, Annaji M, Kurapati S, Dash RP, Srinivas NR, Tiwari AK. Stability-indicating HPLC method for acyclovir and lidocaine in topical formulations. Biomed Chromatogr. 2020;34(3):e4751. doi: 10.1002/bmc.4751, PMID 31756271.
56. Loftsson T, Brewster ME. Pharmaceutical applications of cyclodextrins: basic science and product development. J Pharm Pharmacol. 2010;62(11):1607-21. doi: 10.1111/j.2042-7158.2010.01030.x, PMID 21039545.
57. Shelley H, Babu RJ. Role of cyclodextrins in nanoparticle-based drug delivery systems. J Pharm Sci. 2018;107(7):1741-53. doi: 10.1016/j.xphs.2018.03.021, PMID 29625157.